



ELSEVIER

Contents lists available at ScienceDirect

International Journal of Plasticity

journal homepage: www.elsevier.com/locate/ijplas

Yield surface identification of CP-Ti and its evolution reflecting pre-deformation under complex loading

Ved Prakash Dubey^a, Mateusz Kopec^{a,*}, Magdalena Łazińska^b, Zbigniew L. Kowalewski^a

^a Institute of Fundamental Technological Research, Polish Academy of Sciences, 5b Pawińskiego Str., Warsaw, 02-106, Poland

^b Faculty of Advanced Technologies and Chemistry, Military University of Technology, 00-908 Warsaw, Poland

ARTICLE INFO

Keywords:

Yield surface
Pre-deformation
Plastic anisotropy
Cycle loading, tubular specimen

ABSTRACT

Uniaxial testing methods to characterize materials provide only limited data that is insufficient to fully understand all aspects of their behaviour, such as initial texture or anisotropy. Therefore, this research aims to conduct complex stress loading experiments to understand the physical mechanism accountable for plastic deformation caused by monotonic tension and tension assisted by proportional cyclic torsion in the CP-Ti (Commercially Pure Titanium). The yield surface approach was applied to assess the variation of mechanical properties in the as-received and pre-deformed material. It was found, that such monotonic tension associated with cyclic torsion caused a significant decrease of the tensile stress. The initial yield surface obtained for the as-received material exhibits anisotropic behaviour, whereas, the sizes of subsequent yield surface reflecting pre-deformation were reduced in all directions with exception of the tension direction.

1. Introduction

Titanium and its alloys have been widely used in significant engineering disciplines such as medicine (Alipal et al., 2021), aerospace, and marine engineering (Teschke et al., 2022), due to their high specific strength, corrosion resistance, high impact resistance, and other properties. However, the mechanical testing of these materials is still primarily performed under simple stress conditions in research and commercial facilities. The most common form of testing is tension and compression of solid cylindrical specimens. Such types of testing can only generate limited results concerning the mechanical strength and damage of materials in a single direction which does not simulate the real-world stress conditions encountered by materials in most engineering applications.

In recent years, many researchers have performed complex loadings on metals to investigate their behaviour under metal forming conditions. Combined tension/compression - torsion loading experiments have been conducted on Mg alloys using solid specimens (Shi et al., 2017; Wang et al., 2022) as well as thin-walled tubular specimens (Nazari Tiji et al., 2020; Shi et al., 2022). It should be stressed, however, that solid specimens are not adequate for these experiments since the shear stress and strain distributions along the specimen's radial direction are not uniform. For the rolled Mg alloy AZ31B, the maximum strength is in simple tension (300.1 MPa) and simple compression (297.2 MPa) whereas the lowest strength is in torsion with slight tension (169.3 MPa), and the strength in other loading paths falls in between. This can be attributed to enhanced tension twinning in the tension-torsion loading path (Carneiro et al., 2022). Multiaxial loading tests performed on the sintered porous iron reveal, that strength during uniaxial loading conditions

* Corresponding author.

E-mail address: mkopec@ippt.pan.pl (M. Kopec).

<https://doi.org/10.1016/j.ijplas.2023.103677>

Received 12 March 2023; Received in revised form 13 June 2023;

Available online 15 June 2023

0749-6419/© 2023 The Author(s). Published by Elsevier Ltd. This is an open access article under the CC BY license (<http://creativecommons.org/licenses/by/4.0/>).

was slightly lower than that obtained under combined tension-torsion proportional loading tests with a maximum variation of 10%. Furthermore, the sintered iron exhibited significantly higher strength during non-proportional loading tests in comparison to that captured under proportional loading paths with a maximum aberration of 35%. Such behaviour indicates the presence of additional hardening (Ma et al., 2017). One should highlight, that the evolution of damage in porous sintered metals follows a two-stage process. In the initial stage, plastic deformation primarily occurs at the pore edges, while in the subsequent stage, bulk deformation becomes the dominant mechanism. Notably, micro-cracks always originated from pores orientated with their major axis perpendicular to the direction of tensile loading (Ma et al., 2017; Straffelini and Fontanari, 2011). Commercially pure copper has also been tested under combined tension-torsion loading conditions (Zhao et al., 2017). The results showed, that the magnitude of tensile and shear stresses assessed at a given strain were significantly lower in the combined-loading conditions compared to the simple tension or pure torsion conditions, Fig. 1. The ultimate tensile stress in the simple tension case ($\beta = 90^\circ$) was equal to 274 MPa, whereas, under pure torsion conditions ($\beta = 0^\circ$), shear stress was equal to 160 MPa. One should mention, that for combined loading conditions including tension-dominated loading ($\beta = 49.9^\circ$) and torsion-dominated loading ($\beta = 42.5^\circ$), the tensile stress of 210 MPa and 223 MPa and shear stress of 102 MPa and 141 MPa were obtained, respectively (Zhou et al., 2022). Furthermore, it has been observed, that the simultaneous tension-torsion deformation of pure copper leads to the formation of an ultrafine-grained microstructure with high-angle boundaries. The fractured surface of the specimens subjected to pure torsion exhibited ductile mode with oval cavities. However, under combined tension-torsional loading, the fracture mode transits to a mixed fracture pattern, featuring equiaxial dimples and oval cavities (Li et al., 2014; Zhou et al., 2022).

Fatigue life assessment of different materials had been performed under multi-axial proportional and non-proportional loading conditions (Song et al., 2021; Zhu et al., 2018). Conventional uniaxial fatigue techniques frequently overestimate the fatigue life of engineering components, which might have adverse effects during their critical applications. Over the past few decades, multiaxial fatigue testing has been more important for the goal of a reliable and safe design. Additive manufactured IN718 nickel-based alloy shows slightly lower fatigue lifetimes in the perpendicular to the building direction during tests under combined proportional tension-torsion loading (5295 cycles) than during tension-compression (6081 cycles) and pure torsion (5442 cycles) loading conditions at the equivalent strain amplitude of 1%. It has been found (Jin et al., 2022), that fatigue lifetimes under non-proportional cyclic loading are significantly lower (maximum of 87% decrease) than those in proportional cyclic loading obtained at the same equivalent strain (Jin et al., 2022). Unlike other metals, there have been very limited experimental investigations conducted on Ti and its alloys under complex stress loadings. Majority of these investigations did not involve an effect of the multiaxial loading on the mechanical properties, in particular, yield strength using the concept of yield surface.

Yielding process and strain hardening effect are the primary issues studied in the framework of the material plasticity. An evolution of the initial yield surface well illustrates the characteristics of plastic deformation (Chouksey and Basu, 2021). In order to better understand and describe fairly accurately a mechanical behaviour of the material in question, it is important to carry out the comprehensive experimental investigations of subsequent yield surfaces after different loading histories. A challenge in the initial yield surface determination and its evolution due to deformation history have received much attention in the literature. The yield surface can be described as a region in the stress space where the material always behaves as elastic. The effects of yielding, along with that of isotropic and kinematic hardening, can all be described by using the yield surface. It was found, that various materials exhibited a wide range of shapes of the yield surface in the stress space (Khan et al., 2010a; Kowalewski et al., 2014). The position and shape of the yield surface of a material are substantially impacted by a definition of the yielding, the experimental probe technique (single specimen or multiple identical specimens) used and the loading paths (Iftikhar et al., 2022).

Yield surfaces can be determined by testing a single specimen or multiple identical specimens which are loaded in different stress directions (Iftikhar et al., 2022). Previous experiments show, that results obtained using multiple identical specimens are qualitatively best in comparison to the single specimen technique. It should be mentioned, however, that multiple specimens method for a single yield surface make the experiment costly and machining of geometrically identical testing specimens is nearly impossible (Kowalewski et al., 2001). The disadvantage of single specimen probe technique is the accumulation of additional plastic strain from the previous loading direction on the same specimen. However, this disadvantage can be successfully overcome if loading in one direction is carried

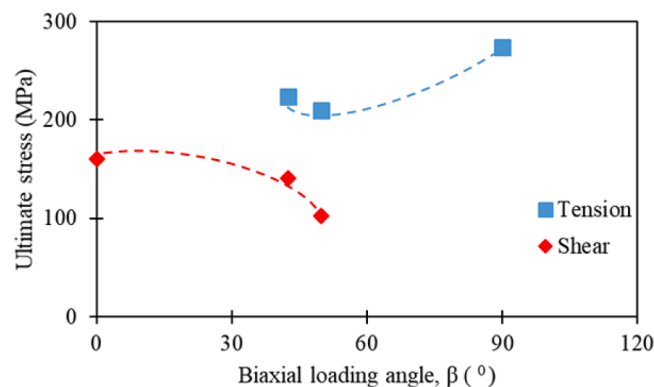


Fig. 1. Variation of the ultimate stress under different states of stress of commercially pure copper (Zhou et al., 2022).

till very limited measurable plastic strain that leads to defining the yield point at small offset plastic strain and also the loading path is following a specific sequence to determine the yield surface.

Researchers have followed different sequences of loading paths to obtain the yield surface amongst which the most preferable are: (1) starting from zero stress level, the specimen is gradually loaded in the tensile direction of a defined stress space and after achieving the desired level of plastic strain, further loading stops and the specimen is unloaded to zero stress level, then this loading-unloading cycle is repeated in the exactly opposite direction of the same offset strain in the stress space defined. The next loading path differs from the previous path by a chosen angular increment (Iftikhar and Khan, 2021); (2) the loading sequence follows a predetermined proportional (or radial) loading path, starting from zero stress, the specimen is first loaded in tension direction only till yielding occurs and then the specimen is completely unloaded and again loaded with some angular increment in the tension-torsion direction of a fixed defined stress space. This loading sequence is carried out till it reaches again the path representing the tension direction only (Dietrich and Socha, 2012). The second sequence is the most suitable for the single specimen technique as previous results obtained using the first one introduces the Bauschinger effect (Holmedal, 2019). The literature review performed in the area of materials and existing methods for yield surface identification enabled to highlight the novelty of this paper, which was mainly expressed by:

- a new database from investigations on CP-Ti alloy carried out under complex stress state;
- complex stress loading experiments to understand the physical mechanism accountable for plastic deformation caused by monotonic tension and monotonic tension assisted by proportional cyclic torsion in the CP-Ti;
- application of the yield surface approach to assess the variation of mechanical properties in the as-received and pre-deformed material;
- identification of the optimal loading parameters under which tension of titanium could be performed under lower forces. This aspect is directly related to the potential applications in the industrial forming processes.
- To the authors' knowledge, there are no such papers available up to now related to the subject presented in the paper. Consequently, yield surfaces were obtained using a single specimen probe technique loaded along the sequential proportional loading paths where yield was defined by the designated offset plastic strain method. Experiments were carried out in order to investigate the yield surface of CP-Ti alloy in the as-received state and its evolution under monotonic tension and various combinations of monotonic tension and cyclic torsion pre-deformation using thin-walled tubular specimens.

2. Materials and methods

The material investigated in this research was CP-Ti alloy. The standard dog-bone solid specimen with a gauge diameter of 6 mm was used for determination of material tensile characteristics under constant strain rate of 0.005 s^{-1} . Test was repeated three times to guarantee the reliability of the results obtained. Further, complex loading tests were performed on the thin-walled tubular specimens. Engineering drawings of the solid and thin-walled tubular specimens are shown in Fig. 2. The wall thickness of the thin-walled tubular specimen is large enough to satisfy the thin-walled tube criterion and to avoid buckling during sequential loading. All the specimens were machined in a Computer Numerical Control (CNC) lathe machine to ensure precise dimensions. The microstructural analysis was performed by using Quanta 3D FEG field emission scanning electron microscope (SEM) operated at 20 kV. The specimens were collected from the central part of the strain gauge area and were prepared by conventional metallographic procedures for titanium, including, grinding, initial polishing and electropolishing. Fig. 2c represents a schematic of the specimen planes [Extrusion direction

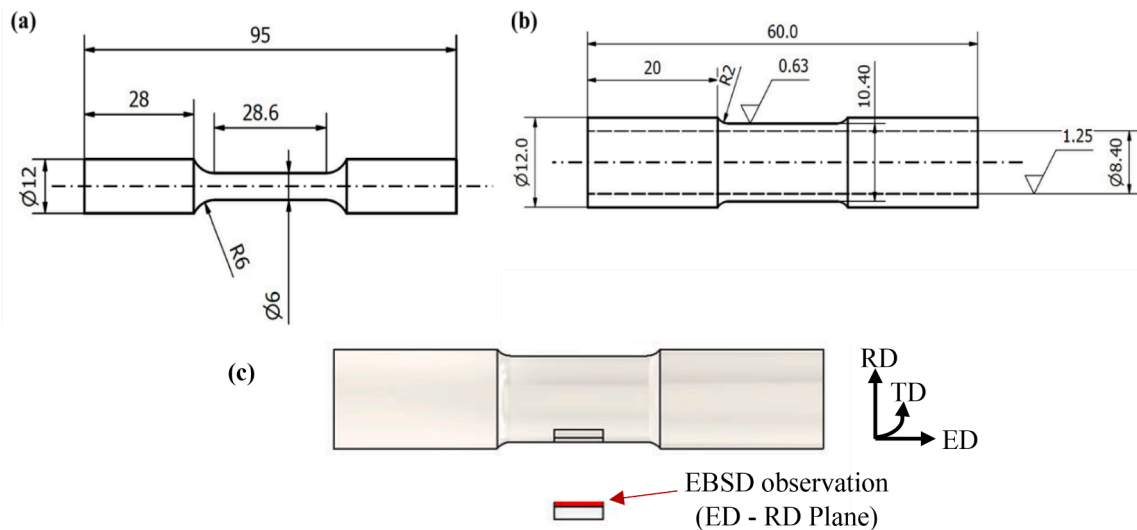


Fig. 2. Engineering drawing of the solid tubular specimen for uniaxial tensile tests (a); and thin-walled tubular specimen (b) for yield surface determination (dimensions in millimeters); scheme of the thin-walled tubular specimen planes for EBSD (c).

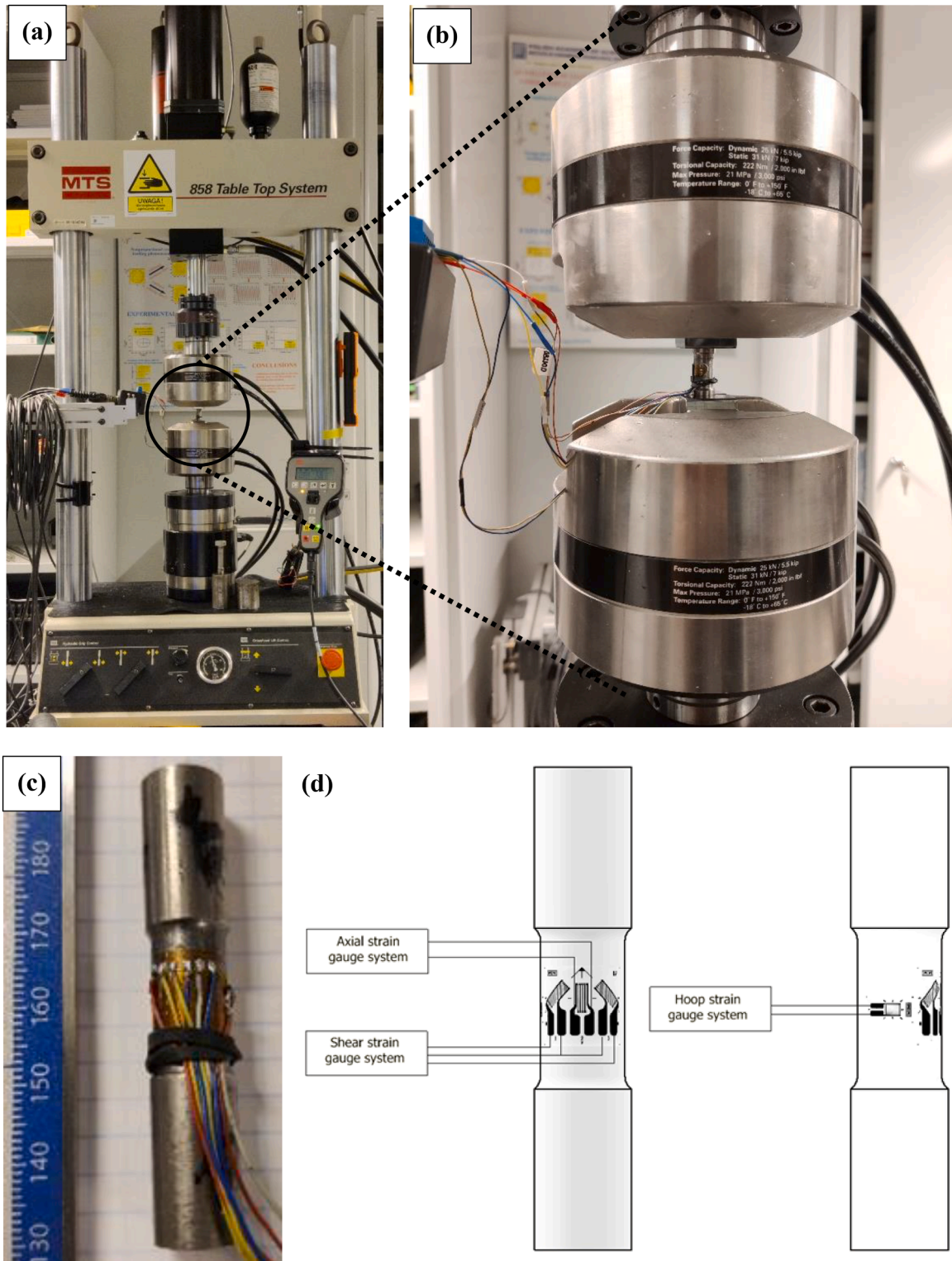


Fig. 3. Set-up of the MTS 858 biaxial testing machine with the strain gauges bonded to the thin-walled tubular specimen (a); and its magnified view (b); image of the strain gauges bonded to the CP-Ti thin-walled tubular specimen (c); schemes of the strain gauge circuits on the specimen (d).

(ED) – Transverse direction (TD) – Radial direction (RD)] of the thin-walled tubular specimen for EBSD observations. In this work, EBSD scan was acquired for ED – RD plane.

The mechanical testing was performed on the MTS 858 biaxial testing machine (Fig. 3a-b) at room temperature (23 °C). Vishay 120Ω temperature compensated strain gauges were bonded on the outer surface of the tubular specimens to measure and control axial, shear and hoop strain, Fig. 3c-d. The axial and shear strain components were measured using three-element 45° rectangular rosette EA-05-125RA-120 with a gauge length equal to 3.18 mm and the hoop strain using linear pattern rosette EA-13-062AK-120 with a gauge length equal to 1.57 mm. Both gages were produced by Vishay. The gages were bonded using M-Bond 610 adhesive produced by Measurements Group Inc. The three-element rectangular rosette was arranged in a manner, that one strain gauge cemented along the longitudinal axis of the specimen was used as the quarter bridge circuit to measure the axial strain, whereas, the other two strain gauges located at +45° and –45° angle with respect to the longitudinal axis of the specimen were used as the half-bridge circuit to measure the shear strain. The hoop strain was measured using a linear rosette by means of the additional half-bridge circuit perpendicular to the longitudinal axis of the specimen. This strain gauges measurement systems enabled independent monitoring of strain. Since they were directly connected to the machine controller, the precise strain control of tests was ensured. Before each test, bridge circuits were calibrated to guarantee the high accuracy of the test.

The experimental programme comprised three essential steps:

- (1) Determination of the initial yield surface of the as-received material;
- (2) Introduction of the following plastic pre-deformation in the specimens:
 - (a) Monotonic tension up to 1% permanent strain under a constant strain rate of $5 \times 10^{-6} \text{ s}^{-1}$.
 - (b) Combination of monotonic tension up to 1% permanent strain under a constant strain rate of $5 \times 10^{-6} \text{ s}^{-1}$, and proportional torsion-reverse-torsion cyclic loading for two magnitudes of strain amplitude (0.2% and 0.4%) at two different values of frequency (0.5 Hz and 1 Hz), Fig. 4.
- (3) Determination of the subsequent yield surfaces of the pre-deformed specimen.

The yield surface concept in the two-dimensional stress space (σ , τ) was applied to identify the impact of plastic pre-deformation on the material by evaluation of the yield points. Yield points were determined by the technique of sequential probes of the single-specimen along different paths in the plane stress state. Starting from the origin, loading in each direction took place until a limited plastic strain was observed (in our case it was 2×10^{-4}). The limited plastic strain of 2×10^{-4} (0.02%) was employed for probing in individual loading paths to ensure, that the plastic offset strain falls within the appropriate range of yield definition assumed. The loading components were strain controlled maintaining a constant ratio of the strain components. Subsequently, the

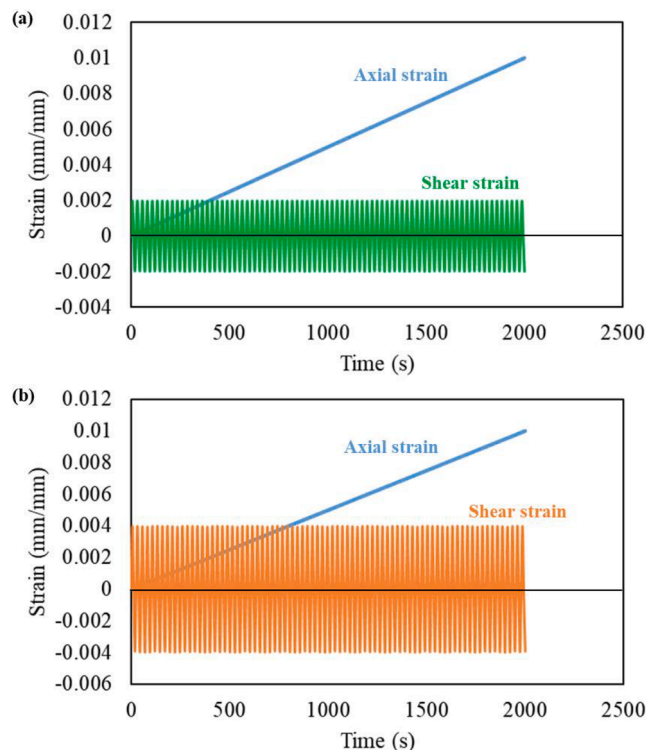


Fig. 4. Strain controlled complex loading programme with monotonic tension and cyclic torsion with strain amplitudes of 0.2% (a); and 0.4% (b) at a frequency of 0.5 Hz.

unloading was carried out under stress control until zero force and torque were reached. The experimental procedure was performed along 17 stress paths (Fig. 5), starting with simple tension and finishing with tension in the same direction. The loading and unloading were carried out for the following strain paths $0^\circ, 30^\circ, 45^\circ, 60^\circ, 90^\circ, 120^\circ, 135^\circ, 150^\circ, 180^\circ, 210^\circ, 225^\circ, 240^\circ, 270^\circ, 300^\circ, 315^\circ, 330^\circ, 360^\circ$ in the $(\epsilon_{xx}, \sqrt{3/(1+\nu)^2}\epsilon_{xy})$ strain plane, Fig. 5. Separate specimens were utilized for each yield surface (initial and pre-deformed) following the aforementioned sequential loading paths, resulting in a total set of six thin-walled tubular specimens. It should be noted, that all specimens after pre-strain in tension or combined tension-torsion were relaxed for 1 hour, and then, subjected to the yield surface determination procedure. By incorporating the relaxation step, it was aimed to limit the effect of different strain rates during pre-deformation and probing since CP-Ti has relatively high strain rate sensitivity.

A selection of the proper methodology to determine yield points in different loading directions is the most important aspect of the yield surface identification procedure. One could distinguish many methods to define the yield point:

- (1) the physical yield point clearly observed on the stress-strain curve (for example stress-strain characteristics of mild steel) (Iqbal et al., 2015);
- (2) a “Designated Offset Strain” represented by a parallel line maintaining the slope of the elastic part of the stress-strain curve drawn at a predetermined offset amount of strain, where the point of intersection between the stress-strain curve and the offset line represents the yield point (Wang et al., 2020);
- (3) a point captured by using “Double Secant Line” method in which two lines are drawn on the stress-strain curve, where one line reflects the elastic deformation behaviour and the other reflects the plastic stage deformation behaviour. The point of intersection of these two secant lines corresponds to the yield point (Zhao and Chen, 2021);
- (4) a point reflecting “Thermoelastic Effect” (specimen temperature is measured during loading condition and the stress corresponding to the minimum of the specimen temperature defines the yield point. It has to be mentioned, however, that this method can only be used for materials having a positive thermal expansion coefficient (Vitzthum et al., 2022).

In this work, the designated offset strain method was used to obtain the yield point since it was found as the most reliable for Ti-like metals, where probes are following a small measurable plastic strain in a loading direction.

One should highlight the importance of careful selection of the plastic offset strain value as a definition of yield point in the yield surface characterization. In several investigations presented in the literature, the plastic offset definition of yield ranging from 0.0005% to 0.2% was often used for determination of the yield surface (Gil et al., 1999; Iftikhar et al., 2021; Ishikawa, 1997; Khan et al., 2009; Phillips and Das, 1985; Tozawa, 1978; Wu and Yeh, 1991). A small plastic offset strain is recommended for the yield definition when only single specimen is used to determine the yield surface. This is due to the fact that the accumulation of additional plastic strain from the previous loading path should be as small as possible to be treated as negligible (Khan et al., 2009). Therefore, to provide a more realistic elastic-to-plastic transition, the yield stress was defined as the effective plastic offset strain equal to 0.01% for each of the loading directions considered. The chosen plastic offset strain definition of yield in this investigation exceeded the 0.001% used in (Khan et al., 2009) due to the selection of a different sequential probing path for yield surface determination. The yield surfaces investigated using these probing parameters showed negligible effect from the history of previous loading paths of the same specimen. The yield surface is formed using yield point values determined for 16 different loading directions in the strain space under consideration (Fig. 5). The last loading path, designated as 17, corresponds to pure tension, and it coincides with the initial loading path, denoted as 1. It was assumed, that 16 different directions of loading in the stress space would be sufficient for determination of a yield

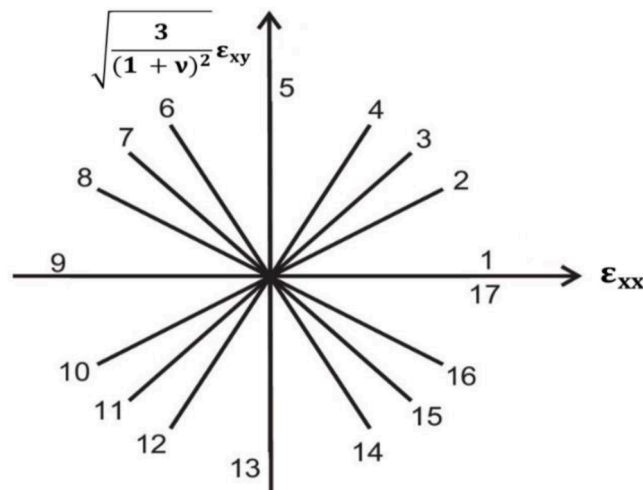


Fig. 5. Loading sequence of strain paths for yield points determination in the biaxial strain space.

surface shape represented by the ellipse.

During all tests, the stress state components were defined by the following well-known relationship for thin-walled tubes:

$$\sigma_{xx} = \frac{4 \times F}{\pi \times (D^2 - d^2)} \quad (1)$$

$$\tau_{xy} = \frac{16 \times T \times D}{\pi \times (D^4 - d^4)} \quad (2)$$

$$\sigma_{eq} = \sqrt{\sigma_{xx}^2 + 3 \times \tau_{xy}^2} \quad (3)$$

$$\varepsilon_{eq} = \sqrt{\varepsilon_{xx}^2 + \frac{3}{(1+\nu)^2} \times \varepsilon_{xy}^2} \quad (4)$$

$$\varepsilon_p = \varepsilon_{eq} - \left(\frac{\sigma_{eq}}{E} \right) \quad (5)$$

$$\vartheta = -\frac{\varepsilon_{yy}}{\varepsilon_{xx}} \quad (6)$$

where, σ_{xx} - axial stress; F - axial force; D - initial outer gauge diameter of the specimen; d - initial inner gauge diameter of the specimen; τ_{xy} - shear stress; T - twisting moment; σ_{eq} - equivalent stress; ε_{eq} - equivalent strain; $\varepsilon_{xx} = E\sigma_{xx}$ - total axial strain; $\varepsilon_{xy} = \tau_{xy}(1+\vartheta)/E$ - total shear strain; ε_p - total plastic strain; E - Young's modulus; ϑ - Poisson's ratio and ε_{yy} - hoop strain.

The Poisson's ratio for the titanium was experimentally determined as the negative value of ratio of hoop (circumferential) to axial (longitudinal) strain values (Eq. (6)). These strains components were precisely recorded by the strain gauges attached to the surface of the specimens gauge length. The average value of the Poisson's ratio was equal to 0.3, and it was simultaneously used in Eq. (5) for a given range of plastic deformation determined for the material in preliminary tests.

The use of Eqns. (1)-(6) was solely intended for controlling the tests in order to obtain a predetermined pre-strain value. It is important to note, that these equations did not have any influence on the actual mechanical response of the material during the loading program, which was the main focus of the study. However, during the experiments, individual components of stress and strain were recorded as the function of time. On their basis, the components of stress are recalculated as functions of the corresponding strain components.

The yield surface is the limit of a region in the stress space where the elastic domain of material behaviour is encompassed (Phillips and Sierakowski, 1965). Thus, when a body transforms from elastic to plastic state, the yield condition gives the best description of the mutual relationship between stresses. Mises yield condition (Mises, 1928) has been used for the isotropic materials in the form $S_{ij}S_{ij} = K^2$, where S_{ij} is the stress deviator and K represents material constant. It should be stressed, however, that materials are not usually isotropic and to study the anisotropic behaviour of materials, yield surface concept belongs to the most effective methods. On the basis of Mises general yield function for crystals (Mises, 1928), Szczepinski has been proposed more general form of the yield function reflecting anisotropy, also reported in the Gol'denblat-Kopnov criterion (Gol'denblat and Kopnov, 1965) and other important effects affecting yield points such as the Bauschinger effect (Szczepinski, 1993). In this paper, such yield condition was applied for the numerical calculation of yield surface.

The experiments were performed in the plane stress conditions, i.e. except of σ_{xx} and τ_{xy} , all other components of stress were equal to zero. The following relationship was derived from Szczepinski anisotropic yield condition for the plane stress state (Szczepinski, 1993):

$$A \times \sigma_{xx}^2 + 2 \times B \times \sigma_{xx} \times \tau_{xy} + C \times \tau_{xy}^2 + 2 \times D \times \sigma_{xx} + 2 \times F \times \tau_{xy} = 1 \quad (7)$$

It represents the second-order curve, where, coefficients A, B, C, D, F can be expressed as following:

$$A = \frac{1}{Y_{xx} \times Z_{xx}} \quad (8)$$

$$B = -k_{16} \quad (9)$$

$$C = \frac{1}{R_{xy} \times S_{xy}} \quad (10)$$

$$D = \frac{1}{2} \times \left(\frac{1}{Y_{xx}} - \frac{1}{Z_{xx}} \right) \quad (11)$$

$$F = \frac{1}{2} \times \left(\frac{1}{R_{xy}} - \frac{1}{S_{xy}} \right) \quad (12)$$

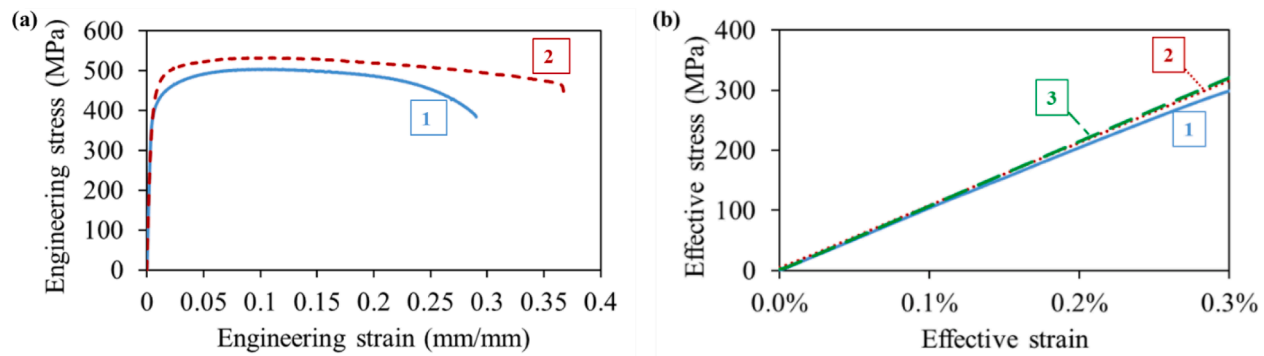


Fig. 6. Tensile stress-strain characteristics of solid tubular (1) and thin-walled tubular (2) specimen of CP-Ti (a); Comparison of material characteristics of pure titanium for different loading paths: simple tension (1); tension-torsion (2) and pure torsion (3) on thin-walled tubular specimen (b).

where, Y_{xx} - yield limit at tension; Z_{xx} - absolute value of yield limit at compression; R_{xy} - shear yield limit for positive value of τ_{xy} and S_{xy} - absolute value of shear yield limit for negative value of τ_{xy} . The coefficient B has no simple physical interpretation, it is proportional to the yield surface rotation in plane stress co-ordinate system (σ_{xx}, τ_{xy}) . In order to define its value, at least one test in the complex stress state is required.

The yield surface for the anisotropic materials can be determined by the five main ellipse parameters, that can be expressed by coefficients of the above mentioned second-order equation in the following way:

(1) Co-ordinates of the ellipse centre:

$$x_0 = \frac{B \times F - C \times D}{\delta} \tag{13}$$

$$y_0 = \frac{B \times D - A \times F}{\delta} \tag{14}$$

(2) Rotation angle of the ellipse axes with respect of (σ_{xx}, τ_{xy}) co-ordinate system:

$$\varnothing = \frac{1}{2} \times \text{atan}\left(\frac{2 \times B}{A - C}\right) \tag{15}$$

(3) Major and minor ellipse semi-axes:

$$a = \sqrt{\frac{\Delta}{a^* \times \delta}} \tag{16}$$

$$b = \sqrt{\frac{\Delta}{b^* \times \delta}} \tag{17}$$

where,

$$\Delta = -A \times C + 2 \times B \times D \times F - C \times D^2 - A \times F^2 - B^2 \tag{18}$$

$$\delta = A \times C - B^2 \tag{19}$$

$$a^* = \frac{1}{2} \times \left(A + C - \sqrt{(A - C)^2 + 4 \times B^2} \right) \tag{20}$$

$$b^* = \frac{1}{2} \times \left(A + C + \sqrt{(A - C)^2 + 4 \times B^2} \right) \tag{21}$$

To fit the experimental data by the equation of ellipse, the least squares method is used to calculate all coefficients of the Eq. (7). As a result of this approach, all values of the coefficients can be calculated, and necessary data regarding the anisotropic properties of the tested material can be captured. One should note, that the Szczepiński anisotropic yield criterion (Szczepinski, 1993) for plane stress (Eq. (7)) can be turned into the von Mises anisotropic yield criterion (Mises, 1928) by imposing $D = F = 0$ and the Hill criterion (Hill, 1948) by imposing $B = D = F = 0$.

3. Results and discussion

3.1. Results of the basic mechanical parameters of the material

The room temperature tensile properties of CP-Ti can be determined on the basis of stress-strain curve (Fig. 6a), they are listed in Table 1. Tensile tests were carried out using solid tubular and thin-walled tubular specimens. The variation of the results obtained in

Table 1
The mechanical properties of CP-Ti.

	0.2% Yield strength [MPa]	Tensile strength [MPa]	Elongation [%]	Young's modulus [GPa]
Solid tubular specimen	390 (± 2)	503 (± 1)	29 (± 0)	107 (± 1)
Thin-walled tubular specimen	400 (± 3)	531 (± 1)	37 (± 1)	100 (± 1)
ASTM standard	350 - 450	> 485	> 28	103

Fig. 6a for both types of specimen was attributed to the specimen geometry differences. It is challenging to compare the findings given here with those in the available literature presented, since the mechanical properties of commercially pure titanium are significantly dependant on the microstructure, interstitial elements (O, N, C) concentration and manufacturing method. As the reference, the yield and tensile strengths published in earlier studies (Attar et al., 2014; Bajoraitis, R., 1988; Bathini et al., 2010; Mouritz, 2012) fall in the ranges of 170–550 MPa and 240–750 MPa, respectively. One can indicate, that the values of these parameters for the material tested are within those ranges.

3.2. Effective mechanical parameters of the material tested under combined loading

Fig. 6b shows the effective stress-strain curve for the comparison of material characteristics determined on the thin-walled tubular specimen subjected to tension (1), tension-torsion (2) and pure torsion (3). It can be observed from the Fig. 6b that all three curves are not very close to each other, i.e. material characteristics varies in different loading conditions for the same material. These differences are probably the result of initial anisotropy introduction to the material during the manufacturing process. This anisotropy will be further discussed in details using the yield surface of ‘as-received’ material in the Section 3.4.

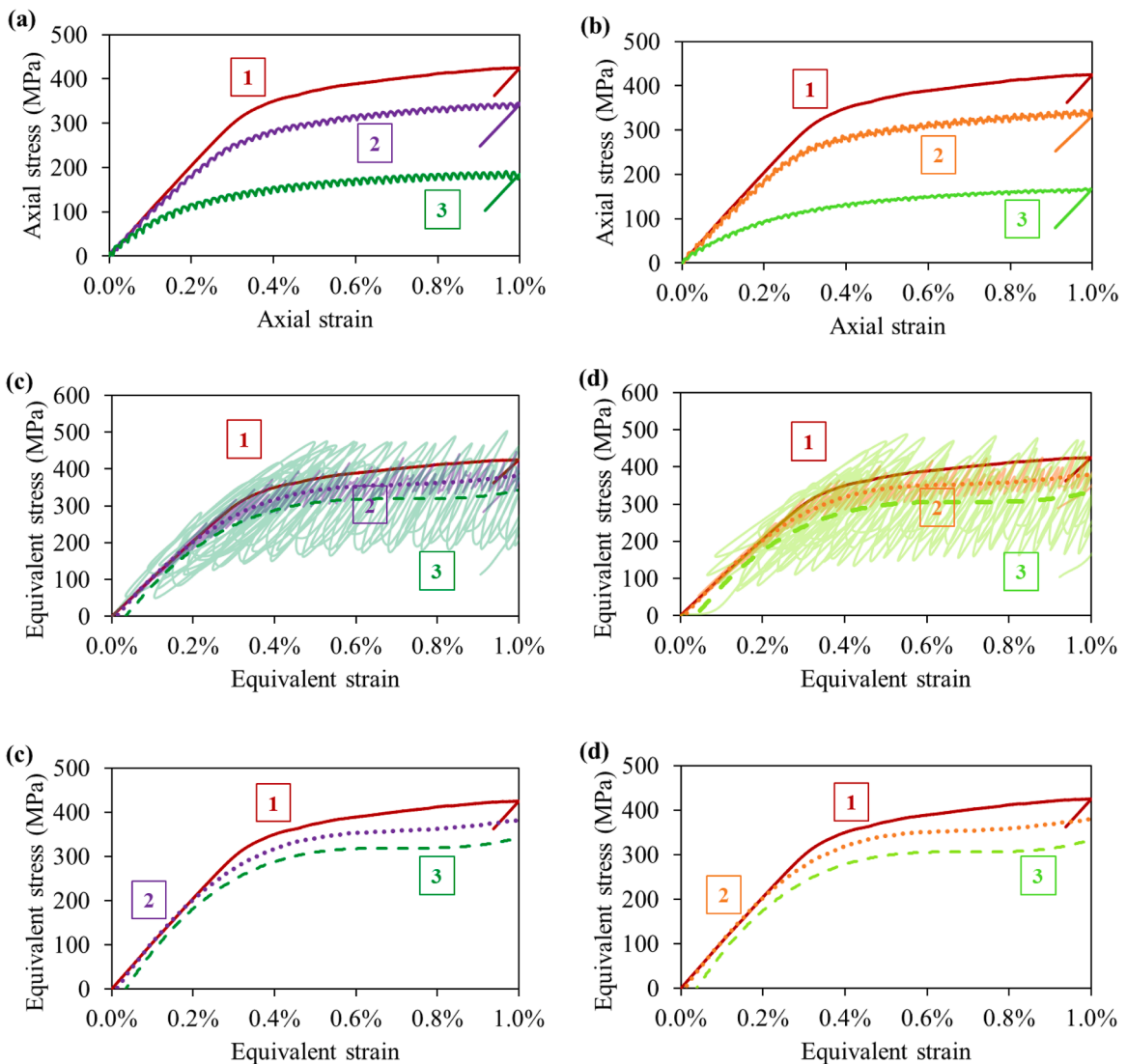


Fig. 7. Comparison of standard tensile curve (1) with tensile characteristics and curves representing equivalent stress captured during monotonic tension assisted by the torsion-reverse torsion cycles of strain amplitude equal to: 0.2% (2) and 0.4% (3) and frequency of: (a, c) 0.5 Hz and (b, d) 1 Hz.

3.3. Results of the material under complex loading

An influence of the cyclic torsion of different strain amplitudes and frequencies on the monotonic tension of CP-Ti was investigated. The main objectives of these tests were to introduce plastic pre-deformation of the material and to investigate variation of the tensile characteristics in the presence of torsion-reverse-torsion cycles. Figs. 7a and 7b clearly show that tensile characteristics of pure titanium significantly varies if tension is associated with cyclic torsion. A tendency of decreasing axial stress, looking like the softening effect, can be clearly observed with the progressive increase of the cyclic strain amplitude. Also, an increase of the frequency led to the decrease of the axial stress. In the case of 0.2% cyclic torsion strain amplitude and frequency of 0.5 Hz, the tensile stress for 0.2% axial strain decreased from 205 MPa to 181 MPa. For the same level of axial strain in the case of cyclic torsion strain amplitude of 0.4% such decrease takes 110 MPa, Fig. 7a. The effect is strengthened for higher value of frequency. The respective values of tensile stress at strain of 0.2% equal to 205 MPa, 178 MPa and 90 MPa, Fig. 7b. The magnitude of axial stress dropped nearly 46% and 56% in the case of frequency equal to 0.5 Hz and 1 Hz, respectively, in comparison to that obtained at tension only for the axial strain equal to 0.2%.

This decrease in tensile stress is expected due to the introduction of shear stress indeed. To address the effect of shear stress on the equivalence of stress in the three cases of loading, Figs. 7c and 7d provide the equivalent stress-strain curves. These curves depict the material's response under different loading conditions. The courses of equivalent stress-strain curves variation clearly demonstrate a softening effect in the material's response as the cyclic torsional strain amplitude increases. This further emphasizes an influence of shear stress on the material's behaviour during simultaneous tension.

The aforementioned tendency of decreasing tensile stress is shown in Fig. 8 for 0.5% axial strain at both cyclic torsion strain amplitude and frequency (Note that the 0% cyclic torsion strain amplitude represents monotonic tension). The same effect has also been reported for Mg-alloy (AZ31B) (Carneiro et al., 2022), commercially pure Cu (Zhou et al., 2022) and aluminium alloy (Al-6061-T6) (Scales et al., 2016) due to typical reduction of the tension twinning volume fraction in Mg alloy and shallow more elongated dimples on Cu fracture surface with the increase of cyclic torsion strain amplitude during combined tension-torsion loading.

3.4. Yield surface of the pure titanium in the as-received state

The yield points describing initial yield surface of CP-Ti were determined by loading-unloading of a single specimen in different strain directions (axial-shear strain) through the specified offset strain method. Fig. 9 shows the pure titanium response in biaxial stress plane on the strain controlled loading program, shown in Fig. 5. It can be observed, that there is negligible deviation from linearity during loading and unloading for each paths. The total plastic strain was equal to 0.02%. The Poisson's ratio for all directions taken into account was equal to 0.3.

A graphical representation of the variation in the effective Young's modulus for the as-received pure titanium specimen under plane stress loading in various directions is shown in Fig. 10. The maximum variation of this parameter is approximately 10%, which emphasizes the existence of texture even for the as-received material. The material texture can be identified by comparison of characteristics determined in all directions considered. CP- metals often exhibit directionality due to preferred texture or crystallographic orientation, as their crystal structures are frequently anisotropic (Omale et al., 2017). In previous studies, it has been reported that the Young's moduli of aluminium and some hexagonal metals, such as titanium and magnesium, exhibit relatively uniform variation compared to other metals such as steels and copper, which exhibit a significant degree of anisotropy (Hutchinson, 2015; Nakajima, 2007). However, the differences in Young's modulus for different directions in plane stress alone do not provide a satisfactory explanation of the initial anisotropy observed in the as-received pure titanium specimen under examination.

Considering the low magnitude of the plastic strain probing involved in the study, such variation of the Young's modulus can have a significant impact on the results of yield surface, if only the Young's modulus of initial elastic curve is used for each stress direction. The authors have performed the experiment while using the initial elastic curve for each direction during plastic strain probing but the obtained results were deemed unacceptable. Specifically, for a limited plastic strain (0.02%) in each direction, which depends on the Young's modulus (Eq. (5)), a lesser equivalent strain was necessary in directions other than the initial direction. The Young's modulus

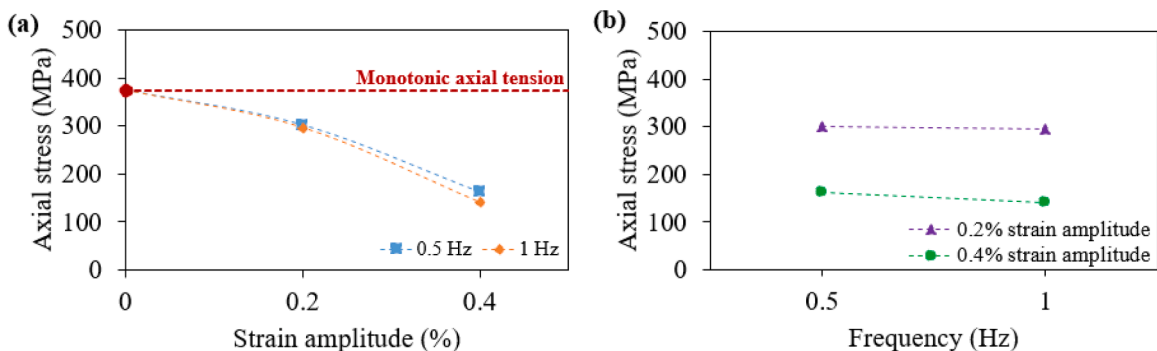


Fig. 8. Variation of the tensile stress corresponding to the 0.5% axial strain value, in response to combined monotonic tension and cyclic torsion of strain amplitude equal to: 0.2% and 0.4% (a) and frequency of: 0.5 Hz and 1 Hz (b).

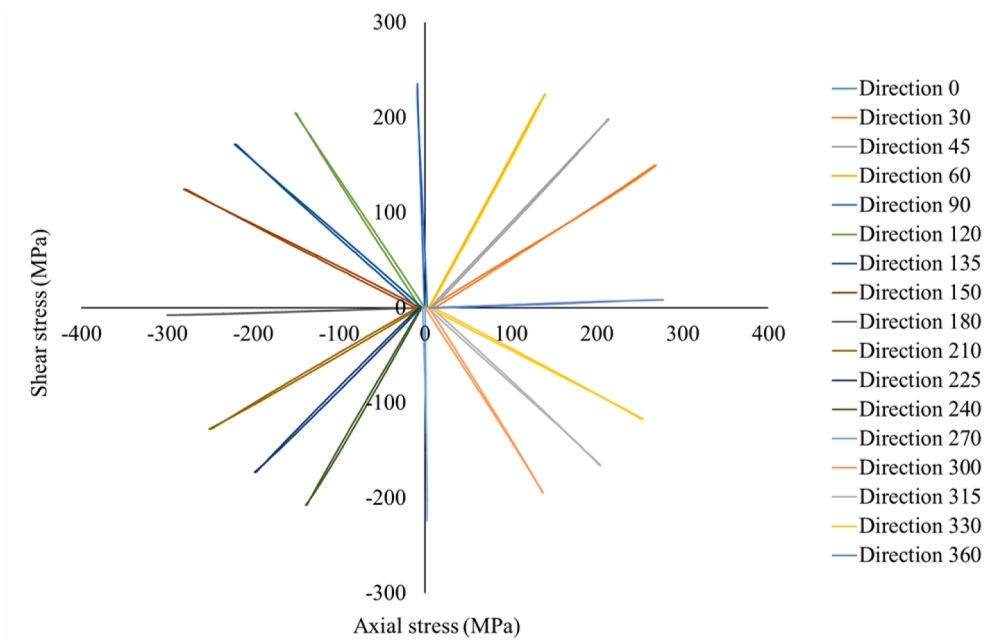


Fig. 9. Stress responses to the strain controlled loading program used for determination of the initial yield surface of CP-Ti.

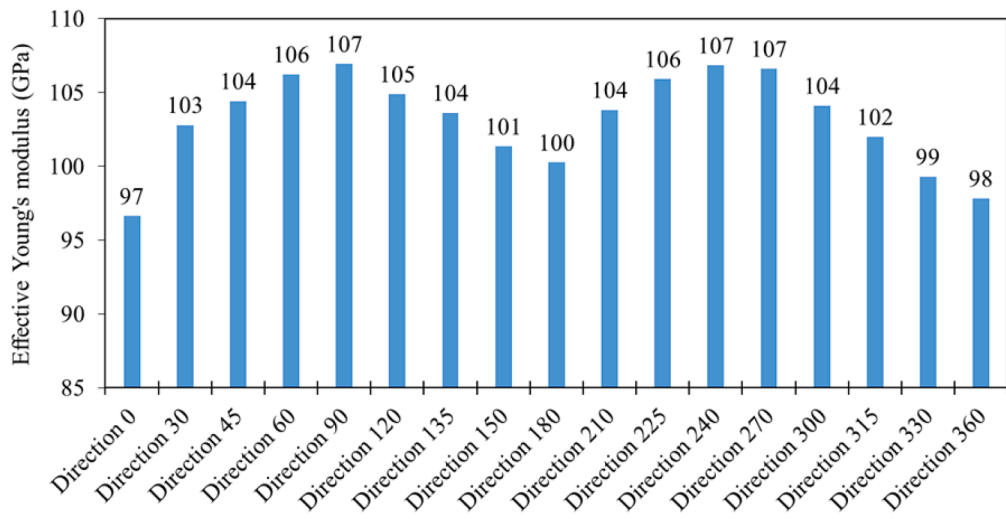


Fig. 10. Variation of the effective Young's modulus in different loading directions in the biaxial strain space for CP-Ti.

obtained for the initial direction is the lowest amongst the directions examined, as shown in Fig. 10. When this variation of the Young's modulus is ignored, the specimen experienced a higher plastic strain in other directions than the pre-defined value. Therefore, to account for the elastic anisotropy in the estimation of plastic strain during probing in different stress directions, the effective Young's modulus specific to each respective direction is utilized. Through this approach, the authors sought to improve the accuracy and reliability of their analysis by considering the elastic anisotropy and its impact on the estimation of plastic strain during probing in various stress directions.

The yield surfaces of the pure titanium in the as-received state were determined using a sequential loading procedure on a single specimen at 0.01% and 0.005% offset strain, as shown by the continuous line and dotted line, respectively, in Fig. 11a. These yield surfaces show the dependence on the chosen definition of yield. After obtaining the yield loci for different directions from experimental results, ellipses were obtained by fitting the A, B, C, D, and F coefficients in Eq. (7) using a least squares evaluation method. The main ellipse parameters for the initial yield surface of the titanium at both selected offset strain values are listed in Table 2. The results for the as-received state of the titanium indicate some level of initial anisotropy, as the yield surfaces are shifted in the compression direction and the axis ratios are significantly lower than 1.73 (the value for an isotropic material according to the von Mises-Huber

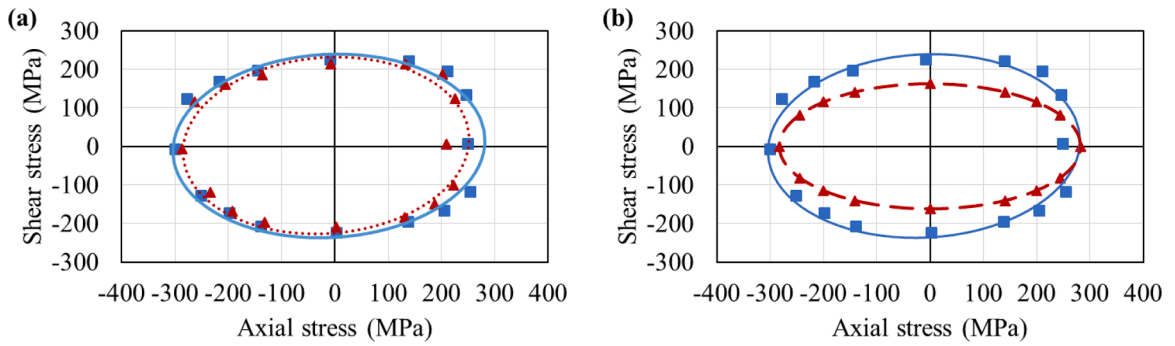


Fig. 11. Yield surface of CP-Ti in the as-received state determined by least square fitting method of yield points (square and triangular points) obtained using a sequential loading technique for two values of plastic offset strain, 0.005% (dotted red line) and 0.01% (continuous blue line) (a); comparison of the initial yield surface (0.01% offset strain) of the CP-Ti (continuous blue line) with the yield surface assuming isotropic material (dashed red line) (b).

Table 2

Five ellipse parameters that define the initial yield surface for CP-Ti.

	Centre (x_0, y_0) [MPa]	Rotation angle (\varnothing) [Radian]	Semi-axes (a, b) [MPa]	Axis ratio (a/b)
0.01% offset strain	-11.36, 1.15	0.14	293.61, 237.11	1.24
0.005% offset strain	-16.82, 1.99	0.22	270.25, 227.17	1.19

yield condition).

In order to compare the yield surface of CP-Ti, an isotropic yield surface was determined by fixing the yield point in tension (direction 0) of the 0.01% offset initial yield surface of pure titanium. The isotropic yield surface was centred at the origin, had a zero rotation angle, and had an axis ratio of 1.73 according to the von Mises-Huber yield criterion. Fig. 11b shows the resulting yield surface. It can be observed from Fig. 11b, that the initial anisotropy present in the material is mainly a distinct hardening behaviour in the shear strength and that is likely a result of the thin-walled tubular specimen manufacturing process from solid specimen or material production process applied to the as-received state of the material.

3.5. Yield surface of the pure titanium in the pre-deformed state

The effect of monotonic tension and complex monotonic tension-cyclic torsion plastic pre-deformation on the mechanical parameters of CP-Ti was assessed based on the evolution of the initial yield surface. All pre-deformations of specimens were carried out until an axial strain of 1% was achieved. Subsequently, the yield surfaces of the pre-deformed specimens were determined using the same procedure as was previously used for the as-received specimen at a 0.01% offset strain.

The yield surface determined for 1% tensile pre-deformed titanium is shown in Fig. 12 as a dashed line. The shape of the yield surface is similar to the initial one, but with an increase in the tensile direction. This indicates that monotonic tensile deformation has induced kinematic hardening of the titanium. The yield point increase in tension is about 45 MPa, which is approximately a 16% greater in comparison to the initial value.

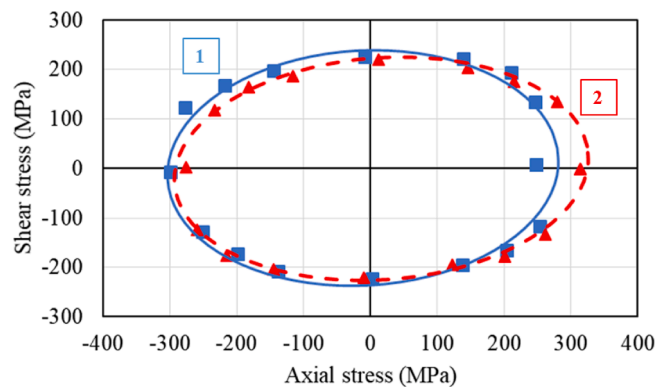


Fig. 12. Comparison of the yield surface for pure titanium after tensile pre-deformation (2) to the initial yield surface (1). Both were obtained at 0.01% offset strain.

Fig. 13 shows the yield surfaces determined after plastic pre-deformation caused by monotonic tension assisted by proportional torsion-reverse-torsion cyclic loading. These yield surfaces are plotted together with the initial yield surface (continuous line) of the material tested. The combined preloading leads to anisotropic hardening of the material. For the torsional strain amplitude of 0.2%, the subsequent yield surface exhibits an increase of the tensile yield and a significant reduction of the compressive yield at frequency of 0.5 Hz (Fig. 13a), which decreases in both directions when the frequency is increased to 1 Hz (Fig. 13c).

On the other hand, for the torsional strain amplitude of 0.4%, the yield surface size of the pre-deformed material is reduced in both the compression and shear directions, but there is an increase in the tensile direction at a frequency of 0.5 Hz (Fig. 13b). However, at an increased frequency of 1 Hz (Fig. 13d), it is interesting to note that the compressive yield is nearly the same as that observed for the initial yield surface, with a further reduction in the shear yield stress. When the frequency is increased from 0.5 Hz to 1 Hz for monotonic tension assisted by cyclic torsion of strain amplitude equal to 0.4%, the higher reduction of shear stress is compensated by an increase of axial stress. One should observed, that regardless the introduced pre-deformation, including monotonic tension and combined tension-cyclic torsion, an increase of the tension stress and a decrease in shear stress at higher torsional strain magnitudes in the titanium could be found. Many studies have been conducted on the effects of pre-deformation on materials, but most of them focus on changes in cumulative mechanical properties (Ghafari and Rezaeepazhand, 2020; Qvale et al., 2021), while only a few researchers have published the results related to changes of directional mechanical properties, specifically using the yield surface evolution approach (Khan et al., 2010a; Kowalewski et al., 2014). Therefore, it is difficult to make an exact comparison to the findings of this work. A similar tendency of pronounced kinematic hardening after 1% tension pre-strain (shown in Fig. 12) was also observed in P250GH and S235JR steel (Stefan et al., 2021) and aluminium alloy (Al 6061-T6511) (Khan et al., 2010b), and it was stated that the existence of incoherent, non-shearable precipitates, which serve as an obstacle to dislocation motion, may contribute to this effect. On the other hand, the evolution of the yield surface after monotonic tension assisted by cyclic torsion was rarely studied by researchers. The yield surface evolution of X10CrMoVnB9-1 steel and Cu 99.9 E copper (Kowalewski et al., 2014) due to combined monotonic tension-cyclic torsion pre-deformation is in good agreement with the findings of this work, as the size of the subsequent yield surfaces is smaller in all the directions except that representing pure tension.

The least squares method was used to calculate the coefficients of the yield equation by fitting the experimental data. The yield surface equation coefficients (A, B, C, D, F) were taken to describe the ellipse representing the approximation yield surface of the tested material. The fitting errors obtained while minimizing the sum of squares of the distances of experimental points from the approximation curve were presented in the Table 3 for each yield surface determined.

The fitting error values obtained for each yield surface were found as minimal, indicating an accurate match between the experimental data and fitted ellipse. Such low fitting errors confirm the suitability, accuracy and reliability of the yield surface equation as well as the quality of the yield surface approximation.

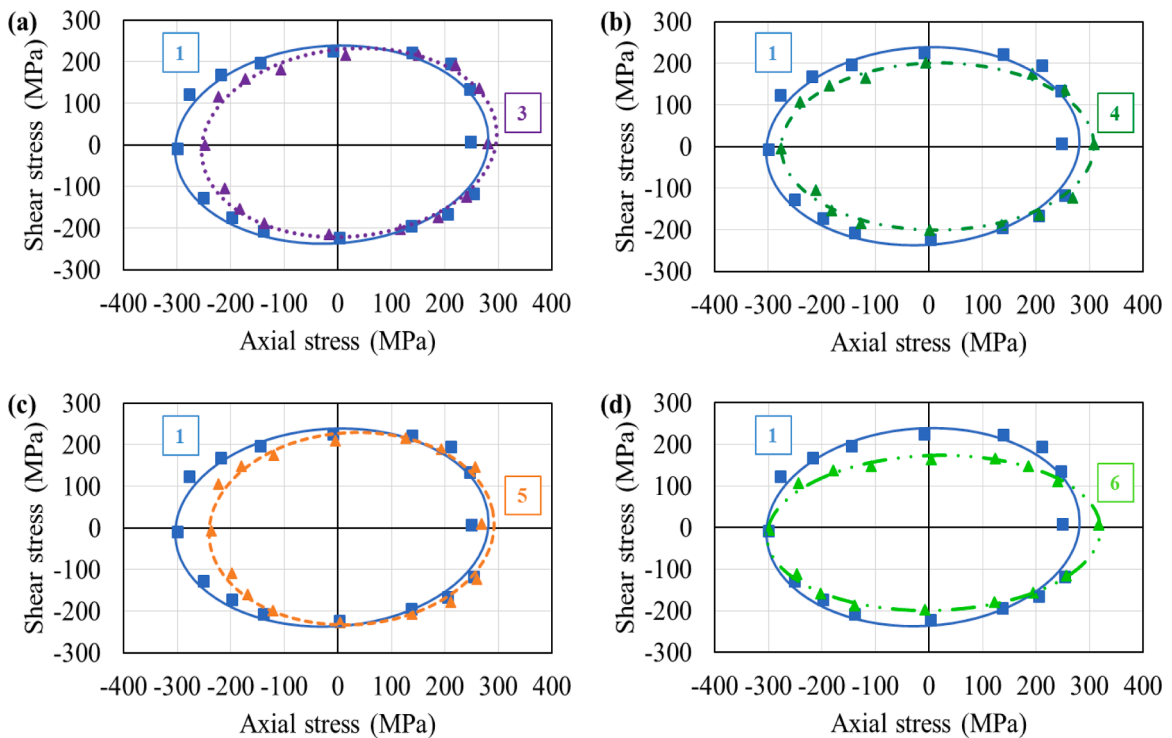


Fig. 13. Comparison of the initial yield surface (1) of CP-Ti to the yield surfaces of pre-deformed titanium due to combined monotonic tension and cyclic torsion of strain amplitude equal to:0.2% (3, 5) and 0.4% (4, 6) and frequency of: 0.5 Hz (a, b) and 1 Hz (c, d), respectively.

Table 3

The fitting errors for the yield surfaces in as-received state and after pre-deformation caused by monotonic tension; combined monotonic tension with cyclic torsion of strain amplitude equal to:0.2% and 0.4% at frequency of: 0.5 Hz and 1 Hz.

As-received	Monotonic tension deformed	0.2% at 0.5 Hz deformed	0.4% at 0.5 Hz deformed	0.2% at 1 Hz deformed	0.4% at 1 Hz deformed
2.31E-01	5.73E-02	1.06E-01	1.07E-01	1.62E-01	5.01E-02

Fig. 14 illustrates the variation in the ellipse parameters that represent the yield surface (YS) of CP-Ti in the pre-deformed state. Pre-deformation caused by monotonic tension is denoted by 0% cyclic torsion strain amplitude. The axes ratio of the yield surface was compared to that representing the initial yield surface (Table 2) and Huber-von Mises-Hencky isotropic yield surface (HMH YS) (1.73) in Fig. 14b and 14e. The results show that the yield surface obtained after monotonic tension assisted by cyclic torsion strain amplitude of 0.4% closely resembles the HMH yield criterion at both frequencies considered (0.5 Hz and 1 Hz). This observation is further supported by the near-zero rotation angle (\emptyset) of the axes with respect of (σ_{xx}, τ_{xy}) co-ordinate system, as shown in Fig. 14c and 14f.

Subsequently, the analysis of the centre of all the yield surfaces was performed (Fig. 15). One should highlight the presence of back stress components which is often observed in materials that have undergone plastic deformation. Fig. 15 shows, that the back stress components are minimal in the as-received state, however, for the pre-deformed state they increased significantly. The back stress arises due to the formation of dislocations, which can block the movement of other dislocations and create areas of high stress in the material.

Fig. 16 depicts a cumulative representation of the evolution of the initial yield surface in the axial-shear stress space that were

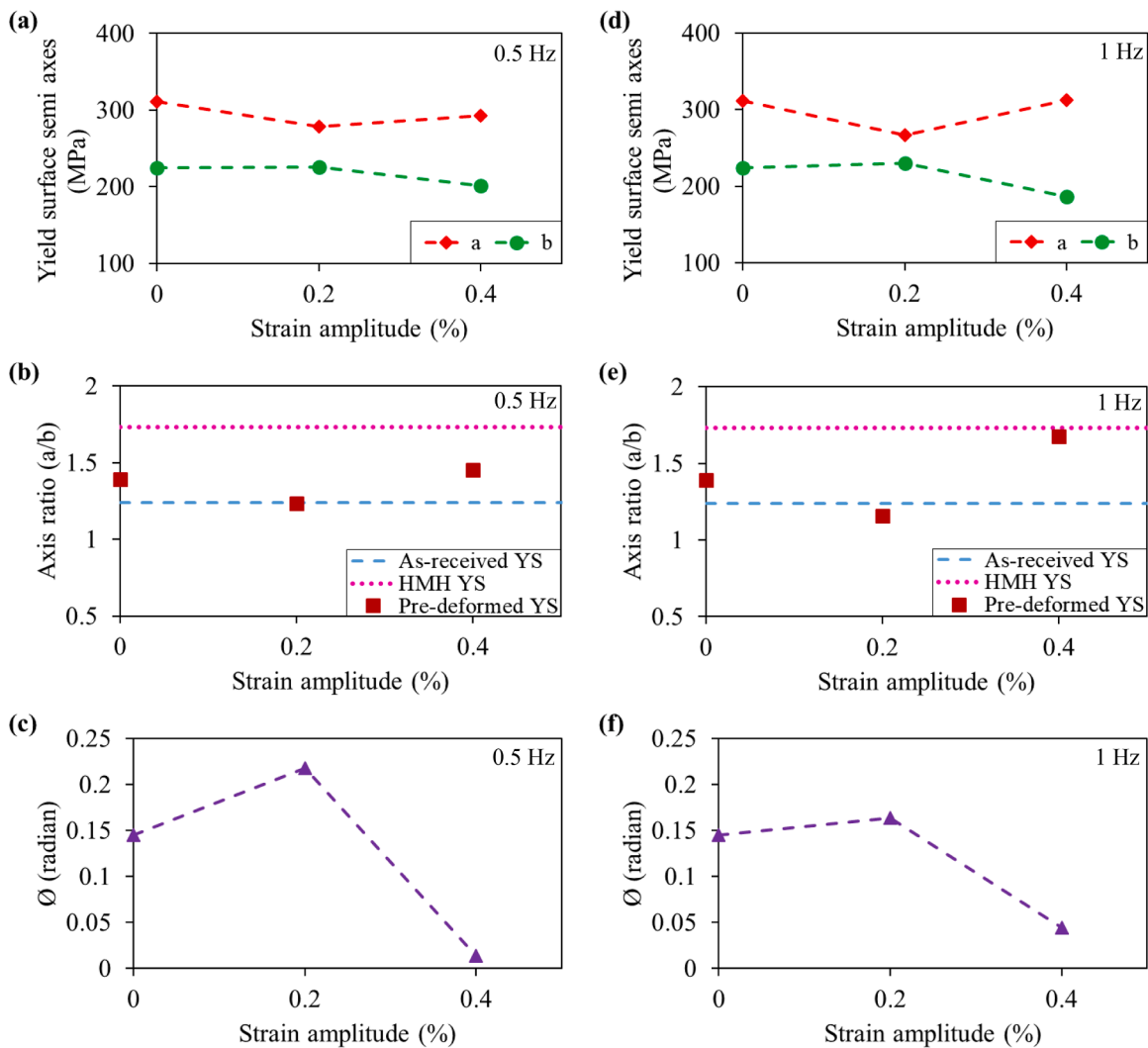


Fig. 14. Variation of the yield surface parameters of CP-Ti due to pre-deformation caused by monotonic tension (0% strain amplitude); combined monotonic tension with cyclic torsion of strain amplitude equal to:0.2% and 0.4% at frequency of: 0.5 Hz (a, b, c) and 1 Hz (d, e, f), respectively.

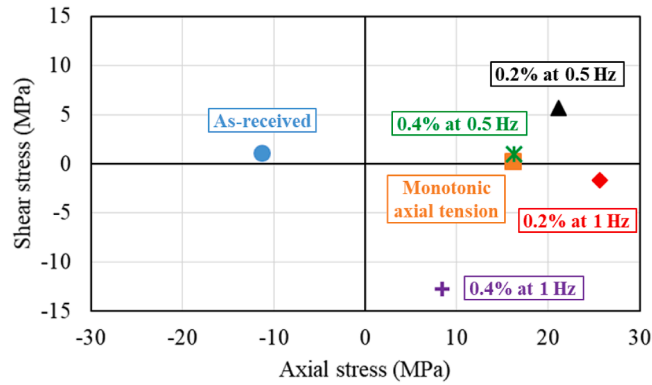


Fig. 15. Analysis of the yield surface origin position of CP-Ti in the as-received state and after pre-deformation caused by monotonic tension; combined monotonic tension with cyclic torsion of strain amplitude equal to:0.2% and 0.4% at frequency of: 0.5 Hz and 1 Hz.

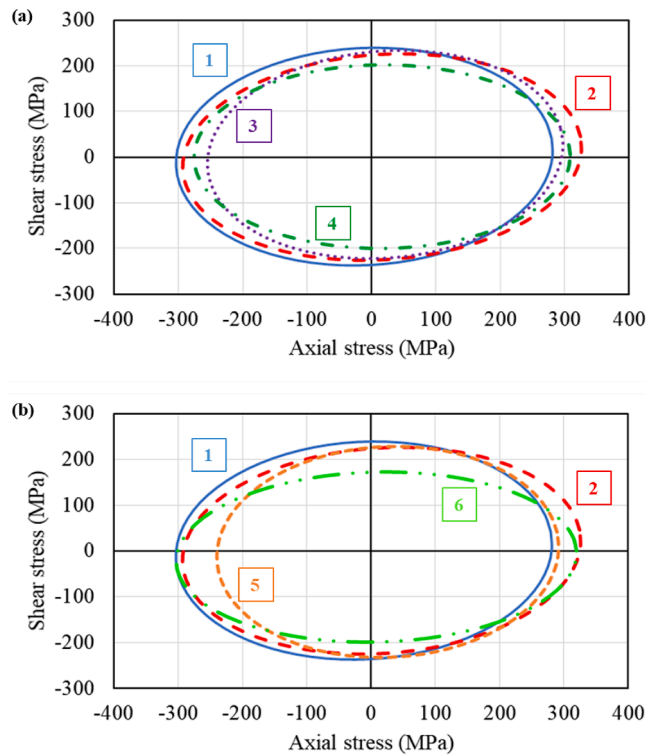


Fig. 16. Evolution of the initial yield surface (1) of CP-Ti due to pre-deformation caused by monotonic tension (2); monotonic tension assisted by cyclic torsion of strain amplitudes equal to: 0.2% (3, 5) and 0.4% (4, 6) at frequencies equal to 0.5 Hz (a) and 1 Hz (b).

obtained from experimental results following pre-deformation of the material at 0.5 Hz and 1 Hz. It can be observed, that the yield surfaces have distinct shapes on the one hand and the size of the subsequent yield surfaces decreases in the direction opposite to the pre-deformation loading on the other. As shown in Fig. 16, the subsequent yield surface for monotonic tension exhibits the largest dimensions. By examining Fig. 16, it becomes evident that the pre-deformed material exhibits both:

- kinematic hardening towards the applied axial pre-deformation direction in comparison to the as-received material surface;
- kinematic softening after the introduction of cyclic torsion during monotonic tensile pre-deformation in comparison to monotonic tensile deformed yield surface.

This is demonstrated by the decrease of subsequent yield loci compared to those for monotonic tensile pre-deformation. For example, the yield surface obtained after combined tension-cyclic torsion with a strain amplitude of 0.2% pre-deformation exhibits a similar shear yield strength but a decrease of axial yield strength compared to that obtained for monotonic tension deformation.

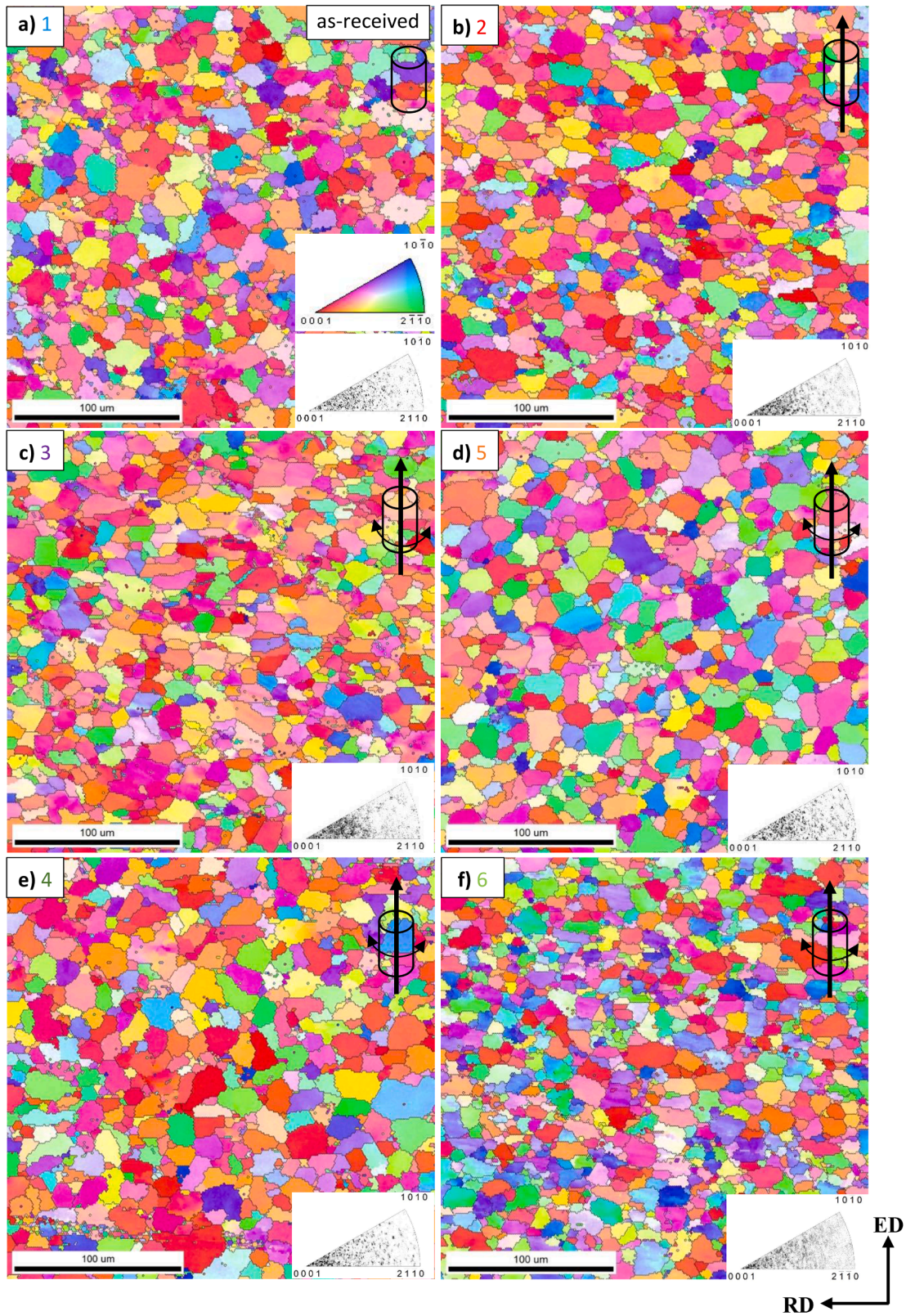


Fig. 17. Inverse pole figure (IPF) maps of the as-received material (a); after monotonic tension to 1% (b); monotonic tension assisted by cyclic torsion of strain amplitudes equal to 0.2% at frequencies equal to 0.5 Hz (c) and 1 Hz (d); and 0.4% at frequencies equal to 0.5 Hz (e) and 1 Hz (f).

Conversely, in the case of combined tension-cyclic torsion with a strain amplitude of 0.4% pre-deformation, the opposite trend is observed. Similar tendencies can be observed for both frequencies of 0.5 Hz and 1 Hz, respectively. The shape analysis of these subsequent yield surfaces reveals that the dimensions of the yield surface are dependant on the preloading direction.

3.6. Microstructural characteristics of the pure titanium in the as-received and pre-deformed state

The microstructure of titanium in its as-received state and its evolution after deformation was presented in the form of Inverse Pole Figure (IPF) maps and (0001) pole figures as shown in Figs. 17 and 18. Each map was related to the specific yield surface presented in Fig. 16. All the specimens were fully recrystallized after the pre-deformation and exhibited similar average grain size. In the as-received state of the material (Figs. 17a and 18a), two ED split basal texture could be observed. The stronger basal texture with most of the c-axes is inclined at $+ (20^\circ - 55^\circ)$ from the TD towards the ED with narrow distribution in the extrusion direction ED-TD plane and a weaker texture component with the c-axes inclined at $- (45^\circ - 60^\circ)$ from TD towards ED. However, with the 1% tensile pre-deformation (Figs. 17b and 18b), both texture component with the c-axis tend to align parallel to the TD as inclination towards the ED decreased maximum of 30° . When material is deformed with combined tension-cyclic torsion with 0.2% strain amplitude (Figs. 17c and 18c), the weaker texture component is intensified and its c-axis aligned more towards the TD. Whereas, the other texture component is weakened. However, with the increase of frequency from 0.5 Hz to 1 Hz (Figs. 17d and 18d), the previous weaker texture component disappeared and a new texture component with the c-axis distributed narrowly in the negative extrusion direction (-ED) – RD plane appears. Simultaneously, the stronger texture component shifts towards negative RD. One could observe a new basal texture with most of the c-axes aligned parallel to the TD and rest distributed in the positive ED-TD plane when pre-deformation caused by combined monotonic tension-cyclic torsion with 0.4% strain amplitude was applied (Figs. 17e and 18e). Whereas, with 0.4% strain amplitude at the frequency equal to 1 Hz (Figs. 17f and 18f), a significantly different grain orientation was observed. The basal texture was distributed widely with the c-axis in the whole ED-TD plane with 3 different high-intensity orientations. First, with most of the c-axes inclined at $- (50^\circ - 68^\circ)$ from the TD towards the ED; second, with the c-axis aligned to be parallel to the TD and third, with the c-axes inclined at $+ (45^\circ - 50^\circ)$ from the TD towards the positive ED-RD plane. These results clearly support the presence of anisotropy and evolution of the initial yield surface of CP-Ti due to pre-deformation, presented in Fig. 16, as texture evolution and preferred grain orientation can be clearly observed in Figs. 17 and 18.

4. Conclusions

In this paper, an experimental approach was performed to investigate the effect of monotonic tension and combined monotonic tension-proportional cyclic torsion on the pure titanium behaviour using the single specimen method. The 0.01% plastic offset strain was adopted as yield definition. Such approach was found to be suitable for sequential probing paths during the yield surface determination. The initial yield surface and its evolution reflecting the pre-deformation history were identified. The main conclusions were drawn as follows:

- Under complex stress states (tension + cyclic torsion), restructurization of the material is responsible for significant decrease of the normal stress. This reduction of the axial stress becomes more prominent with an increase in torsional strain amplitude and frequency.
- The initial yield surface of the as-received titanium for the 0.01% and 0.005% offset strain exhibits anisotropic behaviour and shows clear dependence of yield surfaces on the chosen definition of yield. The manufacturing process of the material or the specimen machining may have caused the initial anisotropy.
- The size of subsequent yield surfaces after pre-deformation of the material were reduced in all directions, except of that representing the pure tension. This indicates, that the introduction of plastic anisotropy caused by the complex loading leads to significant softening in the direction opposite to axial loading.
- CP-Ti exhibits both, kinematic hardening towards the applied tensile pre-deformation direction in comparison to the initial yield surface, and kinematic softening after the introduction of cyclic torsion in monotonic tensile pre-deformation in comparison to monotonic tensile pre-deformed yield surface.
- The low fitting error values obtained for each yield surface after fitting the experimental yield points in the Szczepiński anisotropic yield criterion confirmed the accuracy and quality of the yield surface approximation.
- The analysis of Inverse Pole Figure (IPF) maps and (0001) pole figures reveals a good agreement with the yield response of the as-received and pre-deformed CP-Ti, as texture evolution and preferred grain orientation can be clearly observed in the material.

CRediT authorship contribution statement

Ved Prakash Dubey: Data curation, Formal analysis, Investigation, Methodology, Visualization, Writing – original draft. **Mateusz Kopec:** Formal analysis, Investigation, Methodology, Validation, Visualization, Writing – review & editing. **Magdalena Łazińska:** Investigation, Visualization. **Zbigniew L. Kowalewski:** Conceptualization, Methodology, Project administration, Supervision, Validation, Writing – review & editing.

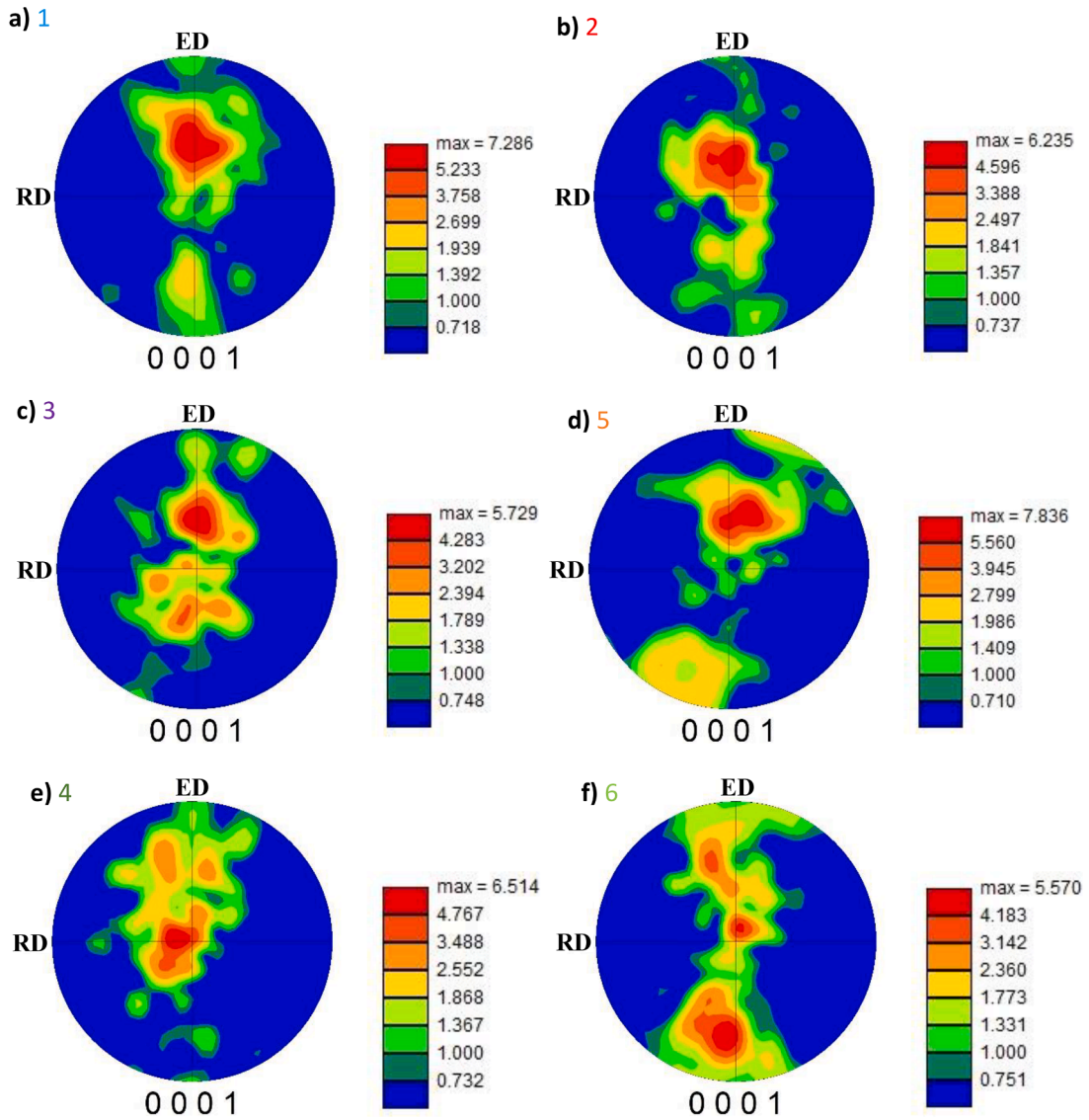


Fig. 18. Pole figure maps of the as-received material (a); after monotonic tension to 1% (b); monotonic tension assisted by cyclic torsion of strain amplitudes equal to 0.2% at frequencies equal to 0.5 Hz (c) and 1 Hz (d); and 0.4% at frequencies equal to 0.5 Hz (e) and 1 Hz (f).

Declaration of Competing Interest

The authors declare that they have no known competing financial interests or personal relationships that could have appeared to influence the work reported in this paper.

Acknowledgements

The authors would like to express their gratitude to the technical staff – Mr M. Wyszowski and Mr A. Chojnacki for their kind help during the experimental part of this work.

This work has been supported by the National Science Centre through the Grant No 2019/35/B/ST8/03151.

References

Alipal, J., Mohd Pu'ad, N.A.S., Nayan, N.H.M., Sahari, N., Abdullah, H.Z., Idris, M.I., Lee, T.C., 2021. An updated review on surface functionalisation of titanium and its alloys for implants applications. *Materials Today: Proceedings, International Conference of Chemical Engineering & Industrial Biotechnology* 42, 270–282. <https://doi.org/10.1016/j.matpr.2021.01.499>.

- Attar, H., Calin, M., Zhang, L.C., Scudino, S., Eckert, J., 2014. Manufacture by selective laser melting and mechanical behavior of commercially pure titanium. *Materials Science and Engineering: A* 593, 170–177. <https://doi.org/10.1016/j.msea.2013.11.038>.
- Bajoraitis, R., 1988. *Forming of Titanium and Titanium Alloys*, 14. ASM Handbook, pp. 838–848.
- Bathini, U., Srivatsan, T.S., Patnaik, A., Quick, T., 2010. A Study of the Tensile Deformation and Fracture Behavior of Commercially Pure Titanium and Titanium Alloy: influence of Orientation and Microstructure. *J. of Materi Eng and Perform* 19, 1172–1182. <https://doi.org/10.1007/s11665-010-9613-5>.
- Carneiro, L., Yu, Q., Jiang, Y., 2022. An experimental study of the mechanical behavior of rolled AZ31B magnesium alloy under combined axial-torsion loading. *Int. J. Plast.* 155, 103319. <https://doi.org/10.1016/j.ijplas.2022.103319>.
- Chouksey, M., Basu, S., 2021. Exploration of subsequent yield surfaces through unit cell simulations. *Int. J. Solids Struct.* 219–220, 11–22. <https://doi.org/10.1016/j.jisolsolstr.2021.02.004>.
- Dietrich, L., Socha, G., 2012. Accumulation of Damage in A336 GR5 Structural Steel Subject to Complex Stress Loading. *Strain* 48, 279–285. <https://doi.org/10.1111/j.1475-1305.2011.00821.x>.
- Ghafari, E., Rezaeepazhand, J., 2020. Isogeometric-based cross-sectional analysis of pre-twisted composite beams. *Thin-Walled Structures* 146, 106424. <https://doi.org/10.1016/j.tws.2019.106424>.
- Gil, C.M., Lissenden, C.J., Lerch, B.A., 1999. Yield of Inconel 718 by Axial-Torsional Loading at Temperatures up to 649 °C. *J. Test. Eval.* 27, 327–336. <https://doi.org/10.1520/jte12233j>.
- Gol'denblat, I.I., Kopnov, V.A., 1965. Strength of glass-reinforced plastics in the complex stress state. *Polymer Mechanics* 1, 54–59. <https://doi.org/10.1007/BF00860685>.
- Hill, R., 1948. A theory of the yielding and plastic flow of anisotropic metals. *Proc. R. Soc. Lond. A* 193, 281–297. <https://doi.org/10.1098/rspa.1948.0045>.
- Holmedal, B., 2019. Bauschinger effect modelled by yield surface distortions. *Int. J. Plast.* 123, 86–100. <https://doi.org/10.1016/j.ijplas.2019.07.009>.
- Hutchinson, B., 2015. Critical Assessment 16: anisotropy in metals. *Mater. Sci. Technol.* 31, 1393–1401. <https://doi.org/10.1179/1743284715Y.0000000118>.
- Iftikhar, C.M.A., Brahme, A., Inal, K., Khan, A.S., 2022. An evolution of subsequent yield loci under proportional and non-proportional loading path of ‘as-received’ extruded AZ31 magnesium alloy: experiments and CPFEM modeling. *Int. J. Plast.* 151, 103216. <https://doi.org/10.1016/j.ijplas.2022.103216>.
- Iftikhar, C.M.A., Khan, A.S., 2021. The evolution of yield loci with finite plastic deformation along proportional and non-proportional loading paths in an annealed extruded AZ31 magnesium alloy. *Int. J. Plast.* 143, 103007. <https://doi.org/10.1016/j.ijplas.2021.103007>.
- Iftikhar, C.M.A., Li, Y.L., Kohar, C.P., Inal, K., Khan, A.S., 2021. Evolution of subsequent yield surfaces with plastic deformation along proportional and non-proportional loading paths on annealed AA6061 alloy: experiments and crystal plasticity finite element modeling. *Int. J. Plast.* 143, 102956. <https://doi.org/10.1016/j.ijplas.2021.102956>.
- Iqbal, M.A., Senthil, K., Bhargava, P., Gupta, N.K., 2015. The characterization and ballistic evaluation of mild steel. *Int. J. Impact Eng.* 78, 98–113. <https://doi.org/10.1016/j.ijimpeng.2014.12.006>.
- Ishikawa, H., 1997. Subsequent yield surface probed from its current center. *Int. J. Plast.* 13, 533–549. [https://doi.org/10.1016/S0749-6419\(97\)00024-7](https://doi.org/10.1016/S0749-6419(97)00024-7).
- Jin, S., Pei, C., Yuan, H., Markert, B., 2022. Multi-axial fatigue life assessment of additively manufactured nickel-based superalloys. *Int. J. Fatigue* 163, 107049. <https://doi.org/10.1016/j.ijfatigue.2022.107049>.
- Khan, A.S., Kazmi, R., Pandey, A., Stoughton, T., 2009. Evolution of subsequent yield surfaces and elastic constants with finite plastic deformation. Part-I: a very low work hardening aluminum alloy (Al6061-T6511). *International Journal of Plasticity, Exploring New Horizons of Metal Forming Research* 25, 1611–1625. <https://doi.org/10.1016/j.ijplas.2008.07.003>.
- Khan, A.S., Pandey, A., Stoughton, T., 2010a. Evolution of subsequent yield surfaces and elastic constants with finite plastic deformation. Part II: a very high work hardening aluminum alloy (annealed 1100 Al). *Int. J. Plast.* 26, 1421–1431. <https://doi.org/10.1016/j.ijplas.2009.07.008>.
- Khan, A.S., Pandey, A., Stoughton, T., 2010b. Evolution of subsequent yield surfaces and elastic constants with finite plastic deformation. Part III: yield surface in tension-tension stress space (Al 6061-T 6511 and annealed 1100 Al). *Int. J. Plast.* 26, 1432–1441. <https://doi.org/10.1016/j.ijplas.2009.07.007>.
- Kowalewski, Z.L., Dietrich, L., Turski, K., 2001. The effects observed in engineering materials after annealing and ageing processes. *J. Mater. Process. Technol.* 165–173. [https://doi.org/10.1016/S0924-0136\(01\)00955-4](https://doi.org/10.1016/S0924-0136(01)00955-4). PART 2: INTERNATIONAL CONFERENCE ON ADVANCES IN MATERIALS PROCESSING TECHNOLOGY 119.
- Kowalewski, Z.L., Szymczak, T., Maciejewski, J., 2014. Material effects during monotonic-cyclic loading. *Int. J. Solids Struct.* 51, 740–753. <https://doi.org/10.1016/j.jisolsolstr.2013.10.040>.
- Li, J., Li, F., Zahid Hussain, M., Wang, C., Wang, L., 2014. Micro-structural evolution subjected to combined tension-torsion deformation for pure copper. *Materials Science and Engineering: A* 610, 181–187. <https://doi.org/10.1016/j.msea.2014.04.083>.
- Ma, S., Markert, B., Yuan, H., 2017. Multiaxial fatigue life assessment of sintered porous iron under proportional and non-proportional loadings. *Int. J. Fatigue* 97, 214–226. <https://doi.org/10.1016/j.ijfatigue.2017.01.005>.
- Mises, R.V., 1928. Mechanik der plastischen Formänderung von Kristallen. *ZAMM - Journal of Applied Mathematics and Mechanics / Zeitschrift für Angewandte Mathematik und Mechanik* 8, 161–185. <https://doi.org/10.1002/zamm.19280080302>.
- Mouritz, A.P., 2012. *Introduction to Aerospace Materials*. Elsevier.
- Nakajima, H., 2007. Fabrication, properties and application of porous metals with directional pores. *Prog. Mater. Sci.* 52, 1091–1173. <https://doi.org/10.1016/j.pmatsci.2006.09.001>.
- Nazari Tiji, S.A., Park, T., Asgharzadeh, A., Kim, H., Athale, M., Kim, J.H., Pourboghrat, F., 2020. Characterization of yield stress surface and strain-rate potential for tubular materials using multiaxial tube expansion test method. *Int. J. Plast.* 133, 102838. <https://doi.org/10.1016/j.ijplas.2020.102838>.
- Omale, J.I., Ohaeri, E.G., Tiamiyu, A.A., Eskandari, M., Mostafajur, K.M., Szpunar, J.A., 2017. Microstructure, texture evolution and mechanical properties of X70 pipeline steel after different thermomechanical treatments. *Materials Science and Engineering: A* 703, 477–485. <https://doi.org/10.1016/j.msea.2017.07.086>.
- Phillips, A., Das, P.K., 1985. Yield surfaces and loading surfaces of aluminum and brass: an experimental investigation at room and elevated temperatures. *Int. J. Plast.* 1, 89–109. [https://doi.org/10.1016/0749-6419\(85\)90015-4](https://doi.org/10.1016/0749-6419(85)90015-4).
- Phillips, A., Sierakowski, R.L., 1965. On the concept of the yield surface. *Acta Mech.* 1, 29–35. <https://doi.org/10.1007/BF01270502>.
- Qvale, K., Hopperstad, O.S., Reiso, O., Tundal, U.H., Marioara, C.D., Børvik, T., 2021. An experimental study on pre-stretched double-chamber 6000-series aluminium profiles subjected to quasi-static and dynamic axial crushing. *Thin-Walled Structures* 158, 107160. <https://doi.org/10.1016/j.tws.2020.107160>.
- Scales, M., Tardif, N., Kyriakides, S., 2016. Ductile failure of aluminum alloy tubes under combined torsion and tension. *Int. J. Solids Struct.* 97–98, 116–128. <https://doi.org/10.1016/j.jisolsolstr.2016.07.038>.
- Shi, B., Peng, Y., Yang, C., Pan, F., Cheng, R., Peng, Q., 2017. Loading path dependent distortional hardening of Mg alloys: experimental investigation and constitutive modeling. *Int. J. Plast.* 90, 76–95. <https://doi.org/10.1016/j.ijplas.2016.12.006>.
- Shi, B., Yang, C., Peng, Y., Zhang, F., Pan, F., 2022. Anisotropy of wrought magnesium alloys: a focused overview. *Journal of Magnesium and Alloys* 10, 1476–1510. <https://doi.org/10.1016/j.jma.2022.03.006>.
- Song, W., Liu, X., Xu, J., Fan, Y., Shi, D., Khosravani, M.R., Berto, F., 2021. Multiaxial low cycle fatigue of notched 10CrNi3MoV steel and its undermatched welds. *Int. J. Fatigue* 150, 106309. <https://doi.org/10.1016/j.ijfatigue.2021.106309>.
- Štefan, J., Parma, S., Marek, R., Plešek, J., Ciocanel, C., Feigenbaum, H., 2021. Overview of an Experimental Program for Development of Yield Surfaces Tracing Method. *Applied Sciences* 11, 7606. <https://doi.org/10.3390/app11167606>.
- Straffelini, G., Fontanari, V., 2011. Stress state dependent fracture behaviour of porous PM steels. *Eng. Fract. Mech.* 78, 1067–1076. <https://doi.org/10.1016/j.engfracmech.2010.12.009>.
- Szczepinski, W., 1993. On deformation-induced plastic anisotropy of sheet metals. *Archives of Mechanics* 45, 3–38.
- Teschke, M., Moritz, J., Telgheder, L., Marquardt, A., Leyens, C., Walther, F., 2022. Characterization of the high-temperature behavior of PBF-EB/M manufactured γ titanium aluminides. *Prog Addit Manuf* 7, 471–480. <https://doi.org/10.1007/s40964-022-00274-x>.
- Tozawa, Y., 1978. Plastic Deformation Behavior under Conditions of Combined Stress. In: Koistinen, D.P., Wang, N.-M. (Eds.), *Mechanics of Sheet Metal Forming: Material Behavior and Deformation Analysis*. Springer US, Boston, MA, pp. 81–110. https://doi.org/10.1007/978-1-4613-2880-3_4.

- Vitzthum, S., Rebelo Kornmeier, J., Hofmann, M., Gruber, M., Maawad, E., Batista, A.C., Hartmann, C., Volk, W., 2022. In-situ analysis of the thermoelastic effect and its relation to the onset of yielding of low carbon steel. *Mater. Des.* 219, 110753 <https://doi.org/10.1016/j.matdes.2022.110753>.
- Wang, E., Sun, G., Zheng, G., Li, Q., 2020. Characterization of initial and subsequent yield behaviors of closed-cell aluminum foams under multiaxial loadings. *Composites Part B: Engineering* 202, 108247. <https://doi.org/10.1016/j.compositesb.2020.108247>.
- Wang, H., Zhang, X., Wu, W., Liaw, P.K., An, K., Yu, Q., Wu, P., 2022. On the torsional and coupled torsion-tension/compression behavior of magnesium alloy solid rod: a crystal plasticity evaluation. *Int. J. Plast.* 151, 103213 <https://doi.org/10.1016/j.ijplas.2022.103213>.
- Wu, H.C., Yeh, W.C., 1991. On the experimental determination of yield surfaces and some results of annealed 304 stainless steel. *Int. J. Plast.* 7, 803–826. [https://doi.org/10.1016/0749-6419\(91\)90019-U](https://doi.org/10.1016/0749-6419(91)90019-U).
- Zhao, B., Chen, W., 2021. Rate-dependent mechanical properties and elastic modulus of ETFE foils used in inflated forming of transparency air-inflated cushion membrane structures. *Engineering Structures* 227, 111404. <https://doi.org/10.1016/j.engstruct.2020.111404>.
- Zhao, C., Li, F., Li, J., Ma, X., Wan, Q., Tong, T., 2017. Influence of Deformation Stress Triaxiality on Microstructure and Microhardness of Pure Copper Processed by Simultaneous Torsion and Tension. *J. of Materi Eng and Perform* 26, 4104–4111. <https://doi.org/10.1007/s11665-017-2797-1>.
- Zhou, J., Xu, Y., Lopez, M.A., Farbaniec, L., Patsias, S., Macdougall, D., Reed, J., Petrinic, N., Eakins, D., Siviour, C., Pellegrino, A., 2022. The mechanical response of commercially pure copper under multiaxial loading at low and high strain rates. *Int. J. Mech. Sci.* 224, 107340 <https://doi.org/10.1016/j.ijmecsci.2022.107340>.
- Zhu, S.-P., Yu, Z.-Y., Correia, J., De Jesus, A., Berto, F., 2018. Evaluation and comparison of critical plane criteria for multiaxial fatigue analysis of ductile and brittle materials. *Int. J. Fatigue* 112, 279–288. <https://doi.org/10.1016/j.ijfatigue.2018.03.028>.